JOURNAL OF PETROLOGY | VOLUME 48 | NUMBER 12 | PAGES 2341–2357 | 2007 | doi:10.1093/petrology/egm062

Classification of Altered Volcanic Island Arc Rocks using Immobile Trace Elements: Development of the Th–Co Discrimination Diagram

A. R. HASTIE[1]*, A. C. KERR[1], J. A. PEARCE[1] AND S. F. MITCHELL[2]

[1]SCHOOL OF EARTH, OCEAN AND PLANETARY SCIENCES, CARDIFF UNIVERSITY, MAIN BUILDING, PARK PLACE, CARDIFF CF10 3YE, UK

[2]DEPARTMENT OF GEOGRAPHY AND GEOLOGY, UNIVERSITY OF THE WEST INDIES, MONA, KINGSTON 7, JAMAICA

RECEIVED OCTOBER 3, 2006; ACCEPTED SEPTEMBER 24, 2007
ADVANCE ACCESS PUBLICATION OCTOBER 25, 2007

Many diagrams conventionally used to classify igneous rocks utilize mobile elements, which commonly renders them unreliable for classifying rocks from the geological record. The K_2O–SiO_2 diagram, used to subdivide volcanic arc rocks into rock type (basalts, basaltic andesites, andesites, dacites and rhyolites) and volcanic series (tholeiitic, calc-alkaline, high-K calc-alkaline and shoshonitic), is particularly susceptible to the effects of alteration. However, by using Th as a proxy for K_2O and Co as a proxy for SiO_2 it is possible to construct a topologically similar diagram that performs the same task but is more robust for weathered and metamorphosed rocks. This study uses >1000 carefully filtered Tertiary–Recent island arc samples to construct a Th–Co classification diagram. A 'testing set' comprising data not used in constructing the diagram indicates a classification success rate of c. 80%. When applied to some hydrothermally altered, then tropically weathered Cretaceous volcanic arc lavas from Jamaica, the diagram demonstrates the presence of a tholeiitic volcanic arc series dominated by intermediate–acid lavas overlain by a calc-alkaline series dominated by basic lavas.

KEY WORDS: *island arc lavas; element mobility; discrimination plots; Jamaica; Caribbean*

INTRODUCTION

The recognized method of classifying most volcanic rocks is the total alkali–silica (TAS) diagram (Le Bas *et al.*, 1986, 1992). The total alkali ($Na_2O + K_2O$) axis mainly distinguishes alkalic from sub-alkalic rock types, whereas the silica axis mainly distinguishes primitive from evolved rock types. This diagram does, however, have limited application to volcanic arc lavas, the vast majority of which simply classify as sub-alkaline. Volcanic arc rocks can be further classified into tholeiitic, calc-alkaline and shoshonitic series. At one time, this was done on the basis of iron enrichment using diagrams such as FeO^{tot}/MgO vs SiO_2 (Miyashiro, 1974; Arculus, 2003) or $(Na_2O + K_2O)$–MgO–FeO^{tot} (the AFM plot of Kuno, 1968). Typically, however, this subdivision is usually made using a K_2O–SiO_2 diagram (Peccerillo & Taylor, 1976; Rickwood, 1989). This diagram has the advantage of assigning both a volcanic series (tholeiitic, calc-alkaline, high-K calc-alkaline, shoshonitic) based mainly on K_2O, and hence the degree of large ion lithophile element (LILE) enrichment, and a rock type (basalt, basaltic andesite, andesite, dacite, rhyolite) based primarily on silica content and hence degree of differentiation.

It has long been recognized that the TAS diagram is not robust in classifying altered volcanic rocks, and proxies using more immobile elements have been developed for that purpose (e.g. Winchester & Floyd, 1977; Pearce, 1996). However, there is no equivalent proxy for the K_2O–SiO_2 diagram, although there have been some efforts in that direction (e.g. Pearce, 1982). The need for a more robust equivalent of that diagram became apparent to us when studying Cretaceous volcanic arc samples from Jamaica, which have undergone hydrothermal alteration followed

*Corresponding author. Telephone: +44 (0)29 208 75874.
E-mail: hastiear@cf.ac.uk

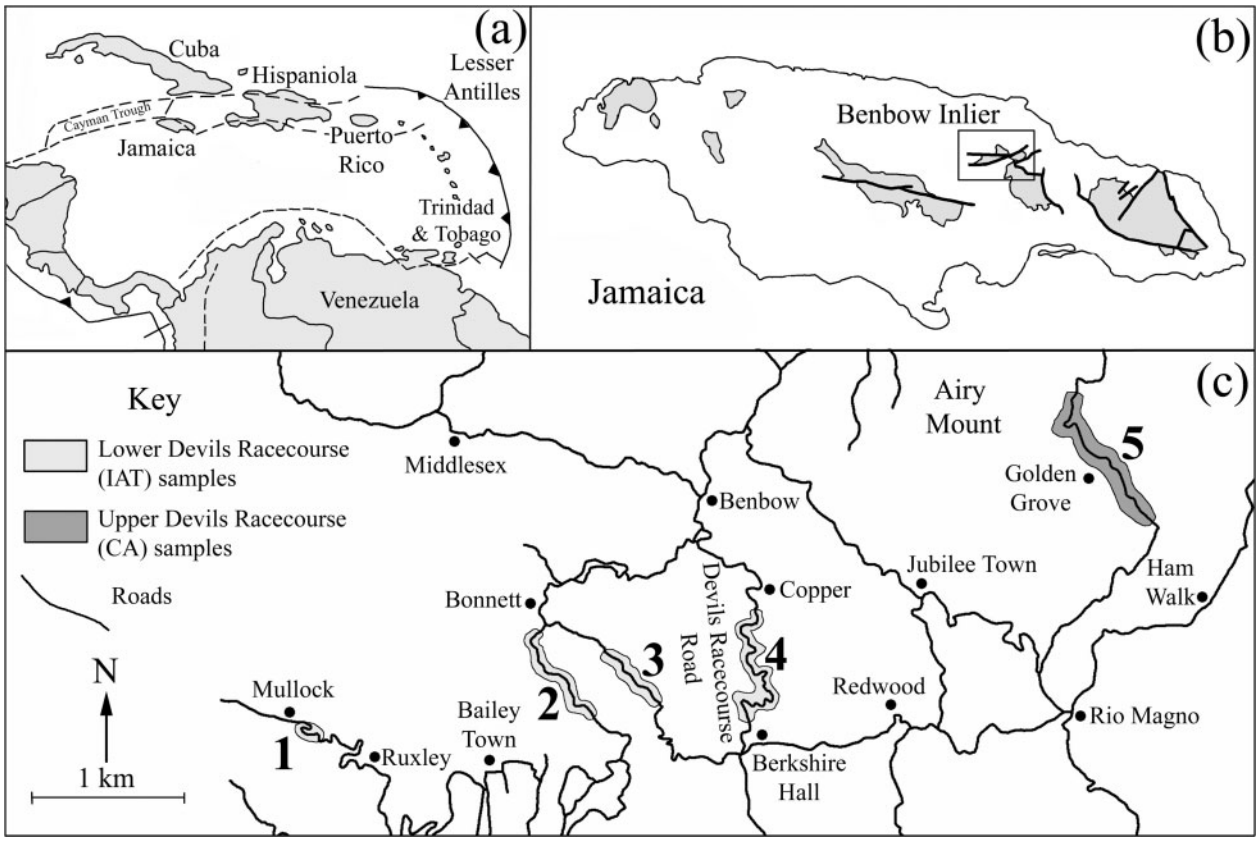

Fig. 1. Simplified maps of (a) the Caribbean region, (b) Jamaica and (c) the Benbow Inlier, locating the Cretaceous arc volcanics of the Devils Racecourse Formation. Samples collected from localities 1–5 in (c) were analysed for a full suite of major and trace elements, providing the data reported in Table 1.

by intense tropical weathering. The aim of this study is to devise a diagram to classify altered volcanic arc lavas on the same basis as the K_2O–SiO_2 diagram and to apply it to the Jamaican samples.

ELEMENT MOBILITY IN METAMORPHOSED AND TROPICALLY WEATHERED ARC ROCKS: THE JAMAICA CASE STUDY

The stimulus for this study was a suite of lower Cretaceous island arc lavas from the Benbow Inlier in eastern Jamaica (Fig. 1). The rocks are part of the Devils Racecourse Formation, which is the oldest lava succession in Jamaica and is composed of ~1000 m of mafic and felsic lavas, volcaniclastic rocks and four interbedded limestone members (Burke *et al.*, 1969).

The succession was split into three sections by Burke *et al.* (1969). The lower section is ~400 m thick; most of the lavas have been silicified. The top 100 m of the lower unit consists of volcanic conglomerates (Burke *et al.*, 1969; Robinson *et al.*, 1972). The middle section consists mainly of volcaniclastic rocks, whereas the upper section is mostly composed of pillow lavas and rare volcaniclastic rocks (Burke *et al.*, 1969; Roobol, 1972).

Twenty-four samples representing the succession have been sampled and analysed for major elements and 30 trace elements by inductively coupled plasma optical emission spectrometry (ICP-OES) and ICP mass spectrometry (ICP-MS) using methods described by McDonald & Viljoen (2006). These data are presented in Table 1 together with international standard values and analytical errors. The lavas are variably porphyritic with plagioclase and clinopyroxene as the dominant phenocrysts, together with oxides in some samples and potassium feldspar in the more silicic rocks. The extent of alteration is also variable, with sericite, chlorite, epidote, calcite, clay minerals and iron oxyhydroxides as the main secondary minerals. This reflects a hydrothermal alteration event post-dated by tropical weathering. The tropical weathering is a particular concern for element mobility, given the high water–rock ratios, high surface temperatures and high concentrations of organic acids (Summerfield, 1997).

Table 1: Major and trace element compositions of the Devils Racecourse lavas, Jamaica

Sample:	AHBI01	AHBI03	AHBI05	AHBI06	AHBI07	AHBI09	AHBI10	AHBI11	AHBI12
Section:	Lower	Lower	Lower	Lower	Lower	Upper	Upper	Upper	Upper
Rock type:	BA/A	BA/A	D/R	D/R	D/R	BA	BA	B	BA
Rock series:	IAT	IAT	IAT	IAT	IAT	CA	CA	CA	CA
Locality:	4	4	4	4	4	5	5	5	5
Major elements (wt %)									
SiO_2	59·07	58·98	81·08	82·63	76·98	50·02	53·85	48·87	45·69
TiO_2	0·86	0·86	0·39	0·30	0·64	1·22	1·17	1·10	1·15
Al_2O_3	15·07	15·04	10·99	10·07	12·62	17·02	16·23	16·96	15·47
Fe_2O_3	8·36	8·39	1·91	0·92	0·91	11·37	7·11	11·14	10·53
MnO	0·14	0·15	0·03	0·01	0·03	0·15	0·11	0·18	0·18
MgO	2·55	2·60	0·84	0·15	2·55	2·96	0·95	3·60	3·66
CaO	2·13	2·40	0·35	0·58	0·39	3·80	6·88	10·66	9·46
Na_2O	7·37	7·10	3·68	3·59	4·39	2·54	5·37	2·79	2·00
K_2O	0·45	0·40	0·16	0·08	0·23	0·61	0·09	0·54	0·31
P_2O_5	0·13	0·12	0·06	0·05	0·14	0·62	0·29	0·16	0·25
LOI	2·24	2·31	1·05	0·69	2·01	7·86	6·99	2·43	9·98
Total	98·38	98·34	100·54	99·07	100·90	98·18	99·03	98·43	98·67
Anhydrous SiO_2	60·42	60·38	81·94	83·21	78·56	54·29	57·89	50·08	50·76
Trace elements (ppm)									
V	151	149	15	10	1	275	251	399	362
Cr	12	16	21	69	17	4	7	30	32
Co	18·7	18·9	3·8	3·7	2·0	23·4	19·9	31·2	24·3
Ni	9	42	5	111	2	8	58	5	10
Ga	15·5	15·7	9·7	7·0	12·6	18·9	11·5	18·1	15·5
Rb	3·75	3·19	0·38	0·20	1·50	2·38	0·28	4·97	0·90
Sr	117	138	43	49	58	435	387	545	467
Y	34·5	31·8	25·7	22·2	34·8	38·6	23·9	21·1	23·8
Zr	82·9	82·1	113·2	96·2	123·3	91·6	86·2	67·1	77·7
Nb	1·86	1·85	1·16	0·93	1·58	2·33	2·17	1·72	1·77
Ba	348	219	414	196	183	469	80	301	657
La	6·25	5·10	6·80	4·80	5·75	23·00	11·00	8·70	9·10
Ce	14·92	12·91	16·92	11·79	16·53	48·31	27·94	20·20	23·78
Pr	2·06	1·98	2·47	1·76	2·85	5·33	4·12	2·82	3·65
Nd	10·41	9·86	11·38	8·66	14·40	23·90	18·12	12·43	16·59
Sm	3·56	3·41	3·00	2·49	4·27	5·40	4·09	3·24	3·94
Eu	1·15	1·13	0·78	0·60	1·05	1·70	1·17	1·12	1·35
Gd	3·93	3·85	3·44	2·82	4·83	5·52	4·02	3·05	3·99
Tb	0·73	0·72	0·56	0·48	0·81	0·82	0·60	0·52	0·59
Dy	5·02	5·01	3·84	3·29	5·70	5·46	3·95	3·41	3·87
Ho	1·02	1·02	0·75	0·64	1·11	1·06	0·75	0·64	0·72
Er	3·04	3·06	2·41	2·11	3·65	3·37	2·39	1·85	2·27
Tm	0·46	0·45	0·38	0·33	0·60	0·51	0·37	0·28	0·35
Yb	3·15	3·23	2·55	2·14	3·94	3·26	2·39	1·92	2·17
Lu	0·49	0·51	0·46	0·40	0·65	0·54	0·40	0·30	0·42
Hf	2·16	2·22	3·12	2·65	3·38	2·63	2·37	1·52	2·14
Ta	0·07	0·08	0·11	0·09	0·11	0·14	0·12	0·06	0·11
Th	0·35	0·34	0·83	0·69	0·65	1·71	1·62	1·17	1·31
U	0·28	0·28	0·50	0·40	0·57	0·48	0·96	0·62	0·59

(continued)

Table 1: Continued

Sample:	AHBI13	AHBI14	AHBI15	AHBI16	AHBI17	AHBI18	AHBI19	AHBI20	AHBI21
Section:	Upper	Upper	Upper	Lower	Lower	Lower	Lower	Lower	Lower
Rock type:	B	BA	BA	BA	D	BA/A	D	D/R	D/R
Rock series:	CA	CA	CA	IAT	IAT	IAT	IAT	IAT	IAT
Locality:	5	5	5	2	2	2	2	2	2
Major elements (wt %)									
SiO_2	52·49	46·12	42·01	53·98	59·44	64·80	65·82	75·73	77·01
TiO_2	1·20	1·17	1·11	1·17	0·97	1·27	0·77	0·39	0·40
Al_2O_3	16·11	14·69	17·53	16·37	14·67	11·57	15·67	11·33	9·51
Fe_2O_3	11·12	13·83	9·16	12·03	9·39	9·85	6·69	3·41	4·56
MnO	0·13	0·24	0·15	0·16	0·20	0·25	0·13	0·03	0·08
MgO	2·65	2·49	3·07	3·35	0·39	2·29	2·28	0·69	1·10
CaO	3·85	6·81	9·86	4·95	4·68	2·27	0·33	1·53	0·50
Na_2O	5·75	4·28	4·12	4·65	5·12	4·53	5·24	1·93	3·32
K_2O	0·25	1·53	0·48	0·18	0·19	0·06	0·05	2·13	0·05
P_2O_5	0·24	0·24	0·24	0·15	0·17	0·25	0·13	0·05	0·08
LOI	5·81	6·95	11·20	2·97	3·54	2·48	2·62	1·96	2·33
Total	99·59	98·35	98·92	99·96	98·75	99·63	99·72	99·18	98·93
Anhydrous SiO_2	55·72	49·57	47·31	55·63	61·62	66·45	67·60	77·25	78·85
Trace elements (ppm)									
V	387	374	325	370	341	320	84	33	15
Cr	12	125	58	23	19	25	29	34	17
Co	30·4	25·0	21·7	31·1	10·2	22·9	9·6	3·5	4·7
Ni	5	30	155	43	34	18	39	32	32
Ga	16·1	17·9	20·5	18·6	11·6	10·8	16·9	10·7	12·8
Rb	2·27	14·48	—	1·04	1·22	0·52	0·51	10·29	0·12
Sr	525	490	689	328	389	112	62	98	32
Y	34·9	22·9	27·1	25·1	21·4	33·7	33·3	42·4	39·7
Zr	89·4	84·3	69·7	49·9	28·9	59·2	74·1	188·2	103·3
Nb	2·14	2·00	1·78	1·25	0·96	1·56	1·56	4·57	1·87
Ba	306	433	143	191	71	99	58	665	29
La	14·50	11·00	13·25	3·08	3·70	4·24	4·17	9·39	6·54
Ce	35·43	25·90	26·01	7·86	8·24	10·53	10·33	22·12	15·53
Pr	5·30	3·52	4·01	1·46	1·10	1·92	1·86	3·58	2·62
Nd	23·31	15·24	16·98	7·56	5·78	9·58	9·06	16·03	12·64
Sm	5·50	3·76	4·17	2·60	2·00	3·16	2·99	4·73	3·92
Eu	1·74	1·30	1·39	1·00	0·80	1·13	0·92	1·01	1·00
Gd	4·99	3·51	4·20	3·24	2·71	3·95	3·66	5·09	4·55
Tb	0·83	0·62	0·67	0·59	0·47	0·72	0·67	0·94	0·84
Dy	5·32	3·90	4·17	3·89	3·16	4·73	4·52	6·35	5·58
Ho	1·01	0·75	0·84	0·78	0·64	0·95	0·96	1·31	1·18
Er	2·95	2·25	2·41	2·29	1·87	2·79	2·91	4·03	3·59
Tm	0·43	0·34	0·36	0·37	0·30	0·45	0·46	0·67	0·59
Yb	2·81	2·24	2·38	2·38	1·90	2·81	3·03	4·64	4·01
Lu	0·45	0·35	0·37	0·35	0·32	0·43	0·47	0·73	0·61
Hf	2·07	2·03	1·84	1·54	0·91	1·68	2·26	5·42	2·90
Ta	0·07	0·07	0·10	0·07	0·05	0·09	0·11	0·33	0·13
Th	1·43	1·41	1·44	0·17	0·09	0·22	0·32	1·50	0·59
U	1·10	0·51	0·75	0·13	0·10	0·15	0·24	0·70	0·50

(continued)

Table 1: Continued

Sample:	AHBI22	AHBI23	AHBI26	AHBI27	AHBI28	AHBI30
Section:	Lower	Lower	Lower	Lower	Lower	Lower
Rock type:	D/R	BA/A	D/R	D/R	D/R	D
Rock series:	IAT	IAT	IAT	IAT	IAT	IAT
Locality:	2	3	3	3	3	1
Major elements (wt %)						
SiO_2	81·42	56·99	77·67	73·22	76·34	66·09
TiO_2	0·31	1·02	0·43	0·53	0·44	0·50
Al_2O_3	8·16	14·59	10·57	12·79	10·59	15·33
Fe_2O_3	1·49	10·22	2·88	4·76	4·14	5·40
MnO	0·02	0·12	0·05	0·04	0·07	0·09
MgO	0·36	1·92	0·43	0·90	0·65	2·44
CaO	0·85	7·45	1·14	0·20	0·24	3·11
Na_2O	2·54	4·47	3·99	5·18	4·73	2·90
K_2O	0·29	0·03	0·06	0·06	0·04	0·72
P_2O_5	0·05	0·12	0·09	0·09	0·09	0·10
LOI	0·98	3·03	1·68	1·98	1·55	2·73
Total	96·47	99·95	98·99	99·77	98·89	99·40
Anhydrous SiO_2	82·23	58·77	78·99	74·70	77·54	67·95
Trace elements (ppm)						
V	26	307	8	6	5	104
Cr	45	44	18	39	39	9
Co	2·4	18·9	2·4	4·0	3·4	10·4
Ni	67	31	23	66	18	21
Ga	6·1	24·2	12·0	17·6	13·1	14·9
Rb	1·04	0·43	0·25	0·64	0·48	2·94
Sr	50	78	56	28	24	136
Y	22·8	22·1	40·4	49·5	34·6	18·5
Zr	97·2	33·3	108·7	145·7	117·9	74·2
Nb	1·34	0·97	2·09	2·71	2·08	1·71
Ba	211	8	264	43	19	700
La	4·35	2·80	6·73	7·31	5·84	4·55
Ce	9·25	6·60	16·02	17·48	15·14	10·07
Pr	1·49	1·17	2·82	3·11	2·63	1·52
Nd	6·70	6·10	13·78	14·47	12·77	6·59
Sm	2·09	2·14	4·17	4·62	3·98	1·86
Eu	0·55	0·91	1·11	1·29	0·86	0·67
Gd	2·45	2·75	4·88	5·65	4·56	2·08
Tb	0·48	0·49	0·90	1·09	0·82	0·39
Dy	3·24	3·29	5·96	7·39	5·47	2·65
Ho	0·70	0·68	1·23	1·53	1·11	0·55
Er	2·17	1·99	3·67	4·64	3·37	1·73
Tm	0·36	0·31	0·57	0·77	0·55	0·30
Yb	2·51	2·04	3·69	5·10	3·63	2·02
Lu	0·41	0·32	0·53	0·74	0·59	0·33
Hf	2·68	1·07	3·28	4·14	3·43	2·04
Ta	0·10	0·06	0·15	0·17	0·15	0·13
Th	0·74	0·11	0·64	0·79	0·66	0·76
U	0·37	0·12	0·51	0·78	0·48	0·46

(continued)

Table 1: Continued

	JB-1a certified values	Av. JB-1a value for this analysis	RSD	Detection limits
Major elements (wt %)				
SiO_2	52·16	52·80	0·86	0·0119
TiO_2	1·30	1·28	2·56	0·0002
Al_2O_3	14·51	14·71	1·45	0·0055
Fe_2O_3	9·10	8·95	1·65	0·0044
MnO	0·15	0·15	3·61	0·0194
MgO	7·75	7·94	1·24	0·0004
CaO	9·23	9·52	2·07	0·0029
Na_2O	2·74	2·58	6·88	0·0029
K_2O	1·42	1·37	6·96	0·0169
P_2O_5	0·26	0·26	2·84	0·0044
Trace elements (ppm)				
V	206	196	2·25	0·07
Cr	415	423	4·26	0·21
Co	39·5	38·1	3·31	0·03
Ni	140	139	7·23	0·34
Ga	18·0	17·9	1·89	0·022
Rb	14	14	91·24	0·031
Sr	443	466	9·32	0·29
Y	24·0	24·0	1·58	0·02
Zr	146·0	137·5	4·86	0·05
Nb	27	28	5·46	0·09
Ba	497	502	2·18	0·41
La	38·1	37·6	3·65	0·011
Ce	66·1	66·4	1·88	0·006
Pr	7·3	7·2	2·14	0·003
Nd	25·5	25·8	1·52	0·006
Sm	5·07	5·12	3·53	0·005
Eu	1·47	1·49	1·44	0·002
Gd	4·54	4·60	3·31	0·028
Tb	0·69	0·68	3·30	0·009
Dy	4·19	4·06	1·67	0·003
Ho	0·72	0·74	2·65	0·001
Er	2·18	2·13	2·59	0·003
Tm	0·31	0·31	2·65	0·001
Yb	2·1	2·07	2·38	0·003
Lu	0·32	0·31	6·44	0·004
Hf	3·48	3·36	5·12	0·002
Ta	1·6	1·6	2·41	0·001
Th	8·8	8·8	3·28	0·002
U	1·6	1·6	9·15	0·004

Major elements determined by ICP-OES; trace elements by ICP-MS. Rock types: B, basalt; BA, basaltic andesite; A, andesite; D, dacite; R, rhyolite. Rock series: IAT, island arc tholeiite; CA, calc-alkaline. RSD, relative standard deviation. The locality numbers refer to Fig. 1. The JB-1a international standard data are based on 10 analyses carried out within the Jamaica analytical run. Detection limits are based on blank analyses. The analytical procedure has been described by McDonald & Viljoen (2006). JB-1a certified values are taken from Govindaraju (1994). LOI, loss on ignition.

The behaviour of an element during weathering and hydrothermal alteration is commonly related to its charge/radius ratio (ionic potential) (e.g. Pearce, 1996). Thus, elements that form ions of low ionic potential ($<0{\cdot}03\ pm^{-1}$) tend to be preferentially removed in solution as hydrated cations, whereas elements forming ions with a high ionic potential ($>0{\cdot}10\ pm^{-1}$) tend to be preferentially removed as hydrated oxyions. Ions of intermediate ionic potential ($0{\cdot}03$–$0{\cdot}10\ pm^{-1}$) tend to remain in the solid product of weathering and so are relatively immobile; this is typically true even at greenschist-grade metamorphism. Thus, the elements Zr, Hf, Nb, Ta, Y, Ti, Cr, the rare earth elements (REE) apart from Eu and possibly La, Th, Ga and Sc are among the most immobile. However, a change in fluid composition from H_2O-rich to a CO_2-rich fluid or SiO_2-rich partial melt, and/or an increase in temperature and/or extremely high fluid throughput may mobilize otherwise immobile elements (e.g. Hynes, 1980; McCulloch & Gamble, 1991; Pearce, 1996; Hill *et al.*, 2000). The mobility of elements in each case must therefore be tested. An effective method is that of Cann (1970), in which an immobile element is plotted on the horizontal axis of bivariate variation diagrams and elements to be evaluated are plotted on the vertical axes. If the two elements are moderately highly incompatible and immobile, and the samples are cogenetic, the data should give trends with slopes close to unity.

For this study, Nb is used as the immobile element (Fig. 2) because it is one of the most immobile (e.g. Cann, 1970; Hill *et al.*, 2000; Kurtz *et al.*, 2000) and has a similar partition coefficient to Th, one of the key elements considered here. Plotting Zr against Nb in Fig. 2a gives a linear trend with a slope of unity for both lower and upper Devils Racecourse lavas, indicating that both elements are immobile and that the variations may be explained by intra-formation differentiation. Figure 2b similarly exhibits significant (95% or better) within-formation correlations, providing evidence for Yb immobility. It also allows the lower and upper units to be distinguished based on their Nb/Yb ratios.

In Fig. 2c, Th similarly exhibits immobile behaviour with two distinct trends, one with high Th/Nb ratios and one with lower ratios. In contrast, in Fig. 2d, U (which is known to be mobile during oxidative alteration) predictably gives a much greater scatter. In Fig. 2e and f, the light REE (LREE), La, and middle REE (MREE), Sm, also give inter-formation correlations consistent with immobility, Sm being more immobile than La.

Significantly for this work, the elements of low ionic potential known to be mobile in most settings (exemplified here by Ba and K), exhibit a large scatter with no evidence of the expected, pre-alteration slope of unity within the lower and upper Devils Racecourse lavas. Clearly, therefore, K has been variably added and/or subtracted during hydrothermal alteration and weathering and is not useful for classifying these rocks; moreover, of the LILE used to identify rock series, Th is likely to be the most robust, although LREE may also be usable in this case.

FINGERPRINTING VOLCANIC ARC ROCK TYPE USING PUBLISHED IMMOBILE ELEMENT DIAGRAMS

Many of the earliest immobile trace element classification diagrams, such as those of Pearce & Cann (1973), Wood *et al.* (1979) and Shervais (1982), focused on fingerprinting the tectonic setting of volcanic rocks. Jackson (1987) used these diagrams to assign an island arc origin to the Devils Racecourse Formation. The normal mid-ocean ridge basalt (N-MORB)-normalized trace element patterns in Fig. 3a clearly highlight the arc-like negative Nb anomalies that characterize all the samples.

Only Floyd & Winchester, in a series of papers (e.g. Floyd & Winchester, 1975, 1978; Winchester & Floyd, 1976, 1977), specifically addressed the identification of rock type. The most commonly used approach is their Zr/TiO_2–Nb/Y diagram (Winchester & Floyd, 1977), which has subsequently been updated using a much larger dataset and statistically drawn boundaries by Pearce (1996) (Fig. 3b). This diagram is essentially a proxy for the TAS classification diagram, where Nb/Y is a proxy for alkalinity ($Na_2O + K_2O$) and Zr/TiO_2 is a proxy for silica. Nb/Y increases from sub-alkalic to alkalic compositions and Zr/TiO_2 increases from basic to acid compositions. The Jamaican samples from the Lower Formation give a wide spread from basalts to dacites or rhyolites, and the Upper Formation plots entirely as basalts (Fig. 3b).

Diagrams such as Fig. 3b, however, have limitations in classifying volcanic arc rocks, as the original Winchester & Floyd (1977) diagram was constructed using all types of igneous rocks except for island arc lavas. This was because of the limited number of analyses of volcanic arc rocks in the 1970s. Thus, the diagrams classify volcanic rocks on the basis of their sub-alkaline and alkaline characteristics but, unlike diagrams such as the Th/Yb–Ta/Yb diagram, cannot subdivide rocks into more specific tholeiitic, calc-alkaline, high-K calc-alkaline and shoshonitic fields (Fig. 3b).

The updated Zr/TiO_2–Nb/Y diagram of Pearce (1996) uses volcanic arc analyses but it raises another problem; namely, the large overlap displayed by island arc basalts, basaltic andesites, andesites and dacites. This overlap is partly because the high water contents of volcanic arc magmas depolymerize the melt creating oxidizing conditions, which causes Fe–Ti oxides to crystallize earlier than in magmas from other tectonic settings. Because melt water content varies between arc volcanoes, Fe–Ti oxide

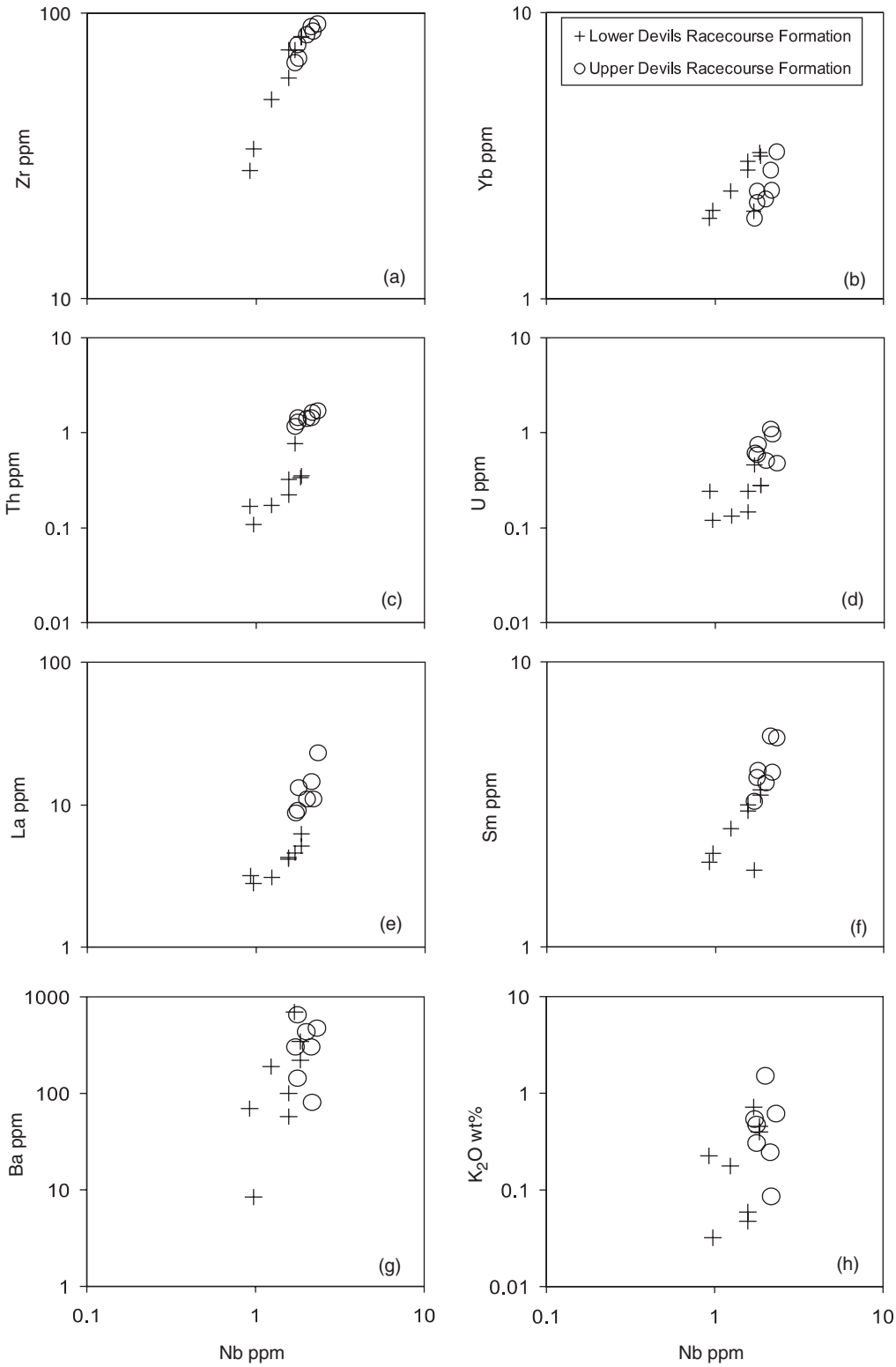

Fig. 2. Variation diagrams for a range of elements plotted against the most immobile element, Nb. In all diagrams, variations within the lower and upper Devils Racecourse Formation at basic–intermediate compositions are mainly due to fractional crystallization, which should give near-diagonal (1:1) vectors on log–log plots. Acid rocks have more complex petrogeneses and have not been plotted.

crystallization, which contributes towards the increase in the silica content of the residual melts, begins at different Zr concentrations and Zr/TiO_2 ratios. In addition, because Zr is more incompatible than Ti, the Zr/TiO_2 ratio is influenced by the degree of partial melting and the processes that cause mantle heterogeneity; it is therefore variable in arc magmas before fractional crystallization takes place. This is true of any ratio using elements of different compatibilities or any element that is moderately to highly incompatible.

To address the problem that the term 'sub-alkaline' does not fully describe all volcanic arc lavas, Pearce (1982) used an 'X'/Yb–Ta/Yb diagram not only to fingerprint arc lavas, but also to identify the volcanic series. The concept is that, in the subduction environment, some elements (including Ta and Yb) will remain in the slab and may be described as 'conservative' whereas others are transferred to the mantle wedge by fluids and/or melts and may be described as 'non-conservative' (Pearce & Peate, 1995). If X is a non-conservative element, volcanic arc data will lie above the MORB array on this type of projection. In addition, the degree of displacement from the MORB array increases from tholeiitic though calc-alkaline to shoshonitic compositions (e.g. Fig. 3c for X = Th). For the Jamaican rocks plotted on this diagram, the Lower Formation plots in the island arc tholeiite field and the Upper Formation plots in the calc-alkaline field (Fig. 3c). However, the use of trace element ratios means that the diagram is largely independent of the effects of fractional crystallization and is able to identify rock series but not rock type. It is thus not the proxy for the K_2O–SiO_2 diagram that is sought here.

CHOICE OF ELEMENTS FOR A K_2O–SiO_2 PROXY DIAGRAM

For a new classification diagram to be constructed, the mobile elements K and, to a lesser extent, Si have to be replaced with immobile elements that behave in a similar way during subduction zone processes, but subsequently remain immobile during surface weathering. The selection of suitable proxy elements requires knowledge of how these elements behave during subduction zone processes.

Replacement of K by a relatively immobile element

The difficulty in finding immobile elements to classify arc volcanic rocks has always been the fact that non-conservative elements have to be mobile at some stage to be driven off the subducting plate. It is now well known from experiment and observation that elements are transferred from the subducting plate to the mantle wedge over different temperature ranges. As the plate subducts, the most fluid-mobile elements such as B and Cs begin to be released at the shallowest depth, then the typical fluid-mobile elements such as K and Ba, and finally the least

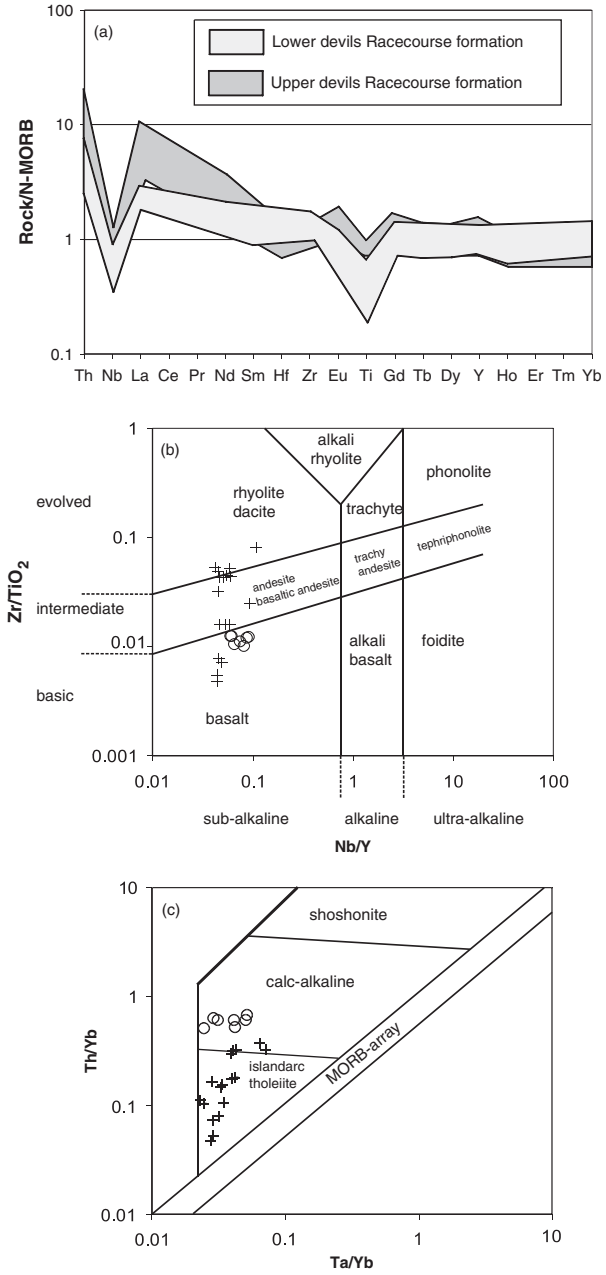

Fig. 3. (a) N-MORB normalized multi-element patterns (given as ranges) highlighting the arc-like character (large negative Nb anomalies) of the lavas of the Lower and Upper Devils Racecourse Formation. Normalizing values in (a) are from Sun & McDonough (1989). (b) Zr/TiO_2–Nb/Y diagram of Pearce (1996) (after Winchester & Floyd, 1977), which is widely used as an immobile element proxy for the TAS diagram. (c) Th/Yb–Ta/Yb ratio plot of Pearce (1982), which provides an immobile element method of identifying arc lavas and their volcanic series. Key as in Fig. 2.

fluid-mobile elements, such as Th and the LREE, begin to be released at still greater depth (e.g. Becker *et al.*, 2000; Savov *et al.*, 2005). This last group provides the only proxies for K in terms of immobility, although their different release profiles mean that they do not behave in precisely the same way. This is apparent in Fig. 2, where Th proves to be the most immobile element that also behaves as a non-conservative element in a subduction context. Thus Th has been chosen to substitute for K in the new classification diagram.

In detail, the mechanism for transport of Th is controversial. A number of studies have used Pb isotopes and other parameters to distinguish two main subduction components: (1) aqueous fluid derived mainly from altered oceanic crust; (2) silicate melts derived mainly from sediment (e.g. Miller *et al.*, 1994; Brenan *et al.*, 1995; Regelous *et al.*, 1997; Class *et al.*, 2000; Elliott, 2003). It is clear that K is mobile in both components but less clear how Th behaves. One view is that it is mobile only in a sediment melt component (e.g. Elliott, 2003), and it is true that experiments indicate a marked increase in Th mobility when the sediment solidus is reached (Johnson & Plank, 1999). On the other hand, these experiments indicate that Th is still mobile, although less so, under subsolidus conditions above 600°C, raising the possibility that Th is also transported by supercritical, subsolidus aqueous fluids. This view has been supported by Keppler (1996), Kessel *et al.* (2005) and others, who have presented convincing experimental evidence that both a 'normal' and a chloride-rich fluid from a subducted slab would readily transport Th into the overlying mantle wedge. However, they too demonstrate decreasing Th mobility with falling temperature. Thus for warm to cool subduction, it is likely that only K is transported by crust-derived fluids at shallow depth, whereas Th and K are transported by sediment melt at greater depth. Between these depths, there is a depth range marked by transport of fluids containing both K and Th but with high K/Th. This is not a problem for the classification provided the shallow and deep subduction components are integrated before they contribute to arc magma genesis.

Viewed from an empirical perspective, various studies have demonstrated Th immobility during tropical weathering: indeed, the immobility of Th in contrast to the mobility of U is the basis for U–Th disequilibria investigations of weathering rates (e.g. Dosseto *et al.*, 2006). Th mobility in metamorphosed crust probably begins in the upper amphibolite facies, so one might infer that it becomes significant at temperatures between about 450 and 650°C. In fingerprinting rocks, this means that it can certainly be treated as immobile in rocks of greenschist facies and below. It also means that a large proportion of the subducted Th will be transmitted to the mantle wedge by the time sub-arc depths are reached. Thus, for the most part, Th can be a proxy for K, even though there are differences in detail in some cases. This is evident in Fig. 4a, where K and Th exhibit near-linear trends in the fresh rocks of modern arcs (Honshu and the Aleutians are shown), even though these may be made up of a range of volcanoes from different locations with respect to the Benioff Zone. However, there is a small component of variation orthogonal to the main trends. This may represent partial decoupling of K and Th during subduction, partial melting effects (K is less incompatible than Th) or some mobilization of K by volcanic fluids. Figure 4a also demonstrates that K mobility causes such relationships to break down entirely in altered equivalents, such as the lavas from Jamaica.

It should be noted that Th/Yb (Fig. 3c) can also be used as a measure of LILE enrichment to discriminate between tholeiitic, calc-alkaline and shoshonitic compositions. There are both benefits and disadvantages in using such a ratio; the advantages are that it reduces the effects of fractional crystallization, plagioclase accumulation and concentration by leaching or dilution by veining. However, the aim here is to provide a proxy for the K_2O–SiO_2 diagram of Peccerillo & Taylor (1976). For that purpose, it is the element that has to replace K_2O, not the ratio.

Replacement of SiO_2 by a relatively immobile element

The most successful immobile element proxy for silica to date has been Zr/TiO_2 (e.g. Winchester & Floyd, 1977). The basis of this ratio is that it mirrors silica by changing little during crystallization of olivine, pyroxene and plagioclase (i.e. within basalts), but increases when Fe–Ti oxides crystallize and help drive the magma composition to more SiO_2-rich compositions. Unfortunately, as noted above, the proxy is only partially effective for volcanic arcs.

In terms of partition coefficients, Si is an element that is slightly incompatible throughout the fractional crystallization and assimilation history of most sub-alkaline magmas. There are no precise immobile element equivalents that we are aware of. Therefore, instead of using an incompatible element we have chosen to use a compatible element, which will be gradually removed from the melt throughout the crystallization sequence and so will reflect fractionation from basalt to rhyolite in an inverse way to silica.

Of the possible candidates, Ni and Cr are too compatible, commonly having values below detection limits in intermediate–acid magmas. Sc is incompatible during melting and slightly to moderately compatible during fractional crystallization, but primary magmas have very variable Sc concentrations because of the variable role of garnet in their genesis (e.g. Pearce & Parkinson, 1993). The most effective trace element, both from a theoretical standpoint and from a series of empirical tests, is Co.

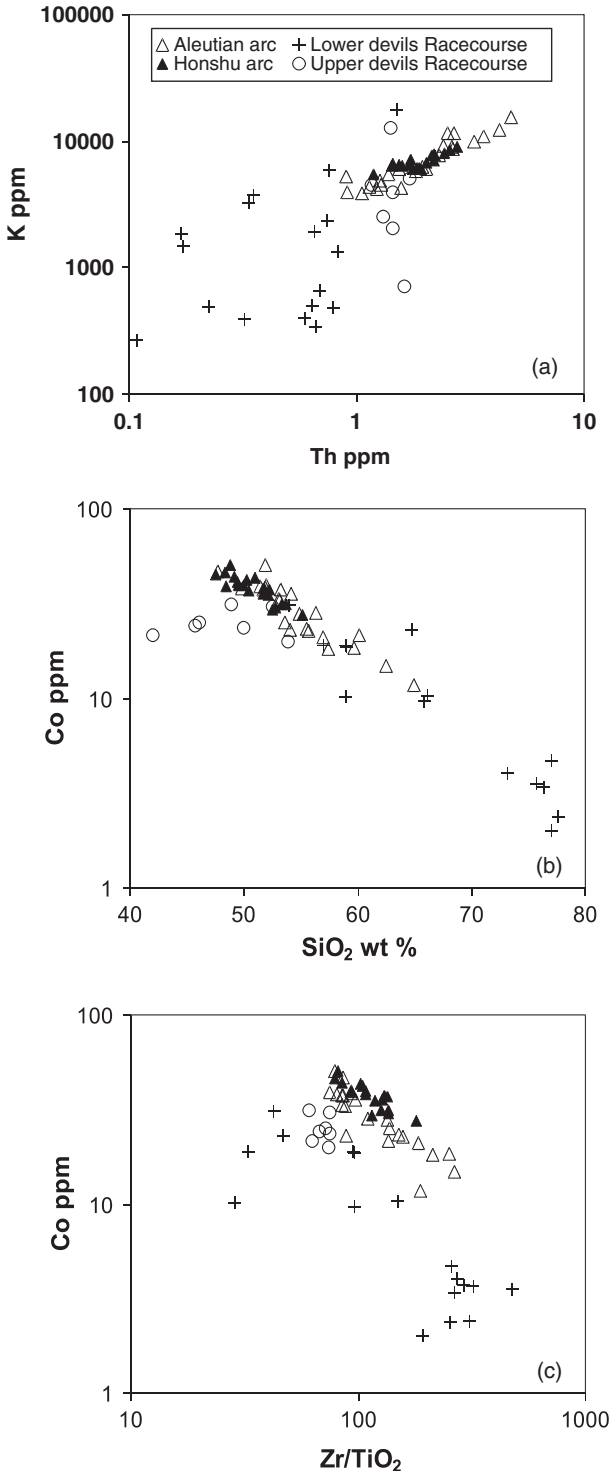

Fig. 4. (a) K–Th, (b) Co–SiO_2 and (c) Co–Zr/TiO_2 variation diagrams for evaluating the immobile element proxies (Th for K, Co and Zr/TiO_2 for SiO_2). The diagram illustrates trends from some typical fresh arc lavas from the Aleutian and Honshu arcs from Nakano (1993, 1994) and Hildreth *et al.* (2004) for comparison with data from the highly altered Jamaica lavas.

Cobalt is partitioned strongly into olivine, which buffers its concentration during partial melting, ensuring little variation between primary volcanic arc magmas. During fractional crystallization, it is highly compatible in olivine and Fe–Ti oxides, slightly compatible with respect to pyroxenes and amphibole, and strongly incompatible with respect to feldspar (Pearce & Parkinson, 1993). For most mineral assemblages, the bulk distribution coefficient is 1·5–2. The Co–SiO_2 variation diagram illustrated in Fig. 4b, again using data from the Aleutian and Honshu arcs, confirms the highly significant inverse correlation between the two elements, providing the basis for Co to be used as a proxy for SiO_2.

For the Jamaican samples, Fig. 4b also shows a good correlation but close examination reveals potential issues. In particular, the Upper Devils Racecourse Formation has a wide range of silica contents (*c.* 42–54 wt %, or 47–58 wt % anhydrous) for little change in Co that would imply a range of rock types from basic to intermediate. However, it is apparent from the Zr/TiO_2–Nb/Y diagram (Fig. 3b) that these samples form a tight cluster, implying that they all belong to a similar rock type. Thus, most of the silica variation apparent in Fig. 4b must be a function of alteration. Using SiO_2 contents recalculated on an anhydrous basis increases the concentrations but retains the variance.

The Co–Zr/TiO_2 diagram (Fig. 4c), comprising the two immobile element proxies, is also informative. Here the Honshu and Aleutian arc examples both form linear trends, the Honshu arc displaced to lower Zr/TiO_2 for a given Co concentration. The Jamaica samples are displaced to still lower Zr/TiO_2 concentrations, probably reflecting the more depleted nature of the source of their primary magmas. The uniform composition of the Upper Devils Racecourse Formation is apparent and alhough a broad negative correlation is evident in the Lower Devils Racecourse data there is more scatter than in the Aleutian and Honshu arc data. In particular, there are two additional trends: one to low Zr/TiO_2 in the more basic samples, and one to low Zr/TiO_2 in the most acid samples. Given that the former samples have Zr/TiO_2 lower than any normal basalts, we interpret this trend in terms of oxide accumulation. The second trend reflects a decrease in Zr concentration in the most silicic rocks and we interpret this in terms of zircon fractionation. Neither oxide nor zircon saturation in the melt has a major impact on Co, making Co potentially a better SiO_2 proxy than Zr/TiO_2. Co does have one potential cause for concern, however: it will increase markedly in response to olivine accumulation. None the less, olivine accumulation also reduces SiO_2, so the olivine accumulation vector is only slightly steeper than the magmatic Co–SiO_2 trend and presents less of a problem for classification.

The immobility of Co is not immediately obvious. Co has two oxidation states, Co^{2+} and Co^{3+} having $\mathcal{Z}/r$ of 0·276 and 0·476 pm^{-1}, respectively, with the result that the former, and dominant, species is potentially mobile and the latter is not. However, one of the principal characteristics of Co that limits its mobility in tropical weathering is its strong adsorption onto iron and manganese oxyhydroxides with accompanying oxidation of Co^{2+} to Co^{3+}. Laterite profiles in ultramafic terranes have long demonstrated that Co immobility accompanies extensive silica loss during tropical weathering (e.g. Trescases, 1973), so Co is an ideal element with which to study the weathered arc lavas from Jamaica. During metamorphism, Co compatibility in Fe-rich minerals such as chlorite, Fe–Ti oxides and amphibole similarly restricts Co mobility. Thus, although care is needed to confirm immobility, Co should be effective in the classification of most altered and metamorphosed rocks.

THE Th–Co CLASSIFICATION DIAGRAM

Compositions of relatively young island arc lavas were taken from the Earth Reference Data and Models database (http://www.earthref.org). The new Th–Co classification diagram was constructed using data from the Tertiary–Recent Aeolian, Aleutian, Andean, Banda, Central American, Honshu, Izu–Bonin, Kamchatka, Kermadec, Lesser Antilles, Luzon, Mariana, New Hebrides, New Zealand, Papua New Guinea, Ryukyu, Sunda and Tonga arcs. Samples designated in the database as being 'weathered' or 'metamorphosed' were removed, as were those with other indices of potential K mobility such as abnormally high water contents or high loss on ignition values. Adakites, boninites, xenoliths, nephelinites and picrites were similarly removed from the dataset to ensure that only basalts, andesites, dacites and rhyolites were used to construct the new classification diagram. Data clearly below cited or estimated analytical resolution limits were also removed. This left 1095 samples with data for both Th and Co that could be used to construct the classification diagram (references are given in Electronic Appendix A, which is available for downloading from http://petrology.oxfordjournals.org). This is the 'training set' (Pearce, 1976).

A second subset of data from two arcs not used in setting up the classification diagram was 'held back' to independently test the effectiveness of the method. This subset is from the Bismarck, Kurile and Aegean arcs and represents the 'testing set' (references are available in Electronic Appendix B, which is available for downloading from http://petrology.oxfordjournals.org).

It should be noted that, despite our efforts to filter the data, the data quality from the Earth Reference Data and Models Database is a slight concern for this study. Predominantly, the filtered Co and Th data are from three analytical methods: more recent ICP-MS, older instrumental neutron activation analysis (INAA), and (for high Th only) X-ray fluorescence (XRF). These methods usually yield reliable data, but we accept that full quality control was not available for all data and thus that the dataset is not internally consistent.

The first step in the construction of the new classification diagram was to plot all the data on the Peccerillo & Taylor (1976) K_2O–SiO_2 diagram, thus allowing all lavas to be labelled according to their degree of differentiation and K enrichment. The distribution of data, plotted to separately emphasize rock type and rock series, is illustrated in Fig. 5.

The arc data, classified on the basis of K_2O and SiO_2 in Fig. 5, were then plotted on the Th–Co diagram (Fig. 6). For each rock type and series, percentage contours were used to construct field boundaries. The contours can be drawn around either the mean or the peak position of the distribution of the data (Le Bas *et al.*, 1992; Pearce, 1996). The Th–Co diagram contained some anomalous samples and therefore the mean values gave erroneous results. Thus, percentage contours were constructed around the peak distribution positions (Fig. 6). Pearce (1996) used the 90% contour to revise the Zr/TiO_2–Nb/Y diagram of Winchester & Floyd (1977), whereas Le Bas *et al.* (1992) used the 75% contour to construct the fields on the TAS diagram. We have arbitrarily chosen the 85% contour for each magma type on the Th–Co diagram (Fig. 6).

The success of the Th–Co diagram as a proxy for the Peccerillo & Taylor (1976) K_2O–SiO_2 diagram can be demonstrated by classifying the samples used to devise the diagram (i.e. the 'training set'). Table 2 gives the results. Classifying according to magma series gives a success rate just above 80% for tholeiitic and calc-alkaline samples. However, the boundary between the calc-alkaline and the high-K calc-alkaline and shoshonitic lavas has a lower success rate of 78%. In part, this is because of the lack of samples and the lack of a reliable distribution peak. In particular, it should also be noted that the numbers of samples for trachyte and latite in the database were extremely small, which may necessitate revision of these fields as more data become available. Classifying according to rock type (basalt, basaltic andesite–andesite, dacite–rhyolite) gave an average success rate of 77%, the biggest overlap being between basalt and basaltic andesite–andesite rock types. Table 2 also shows that the 'testing set' of samples from the Bismarck, Kurile and Aegean island arcs has an overall success rate of >80% for both the magma series and rock type classification, similar to that of the 'training set'.

There are many reasons why the success rate is not greater than 80%. Analytical errors in the determination of Th and

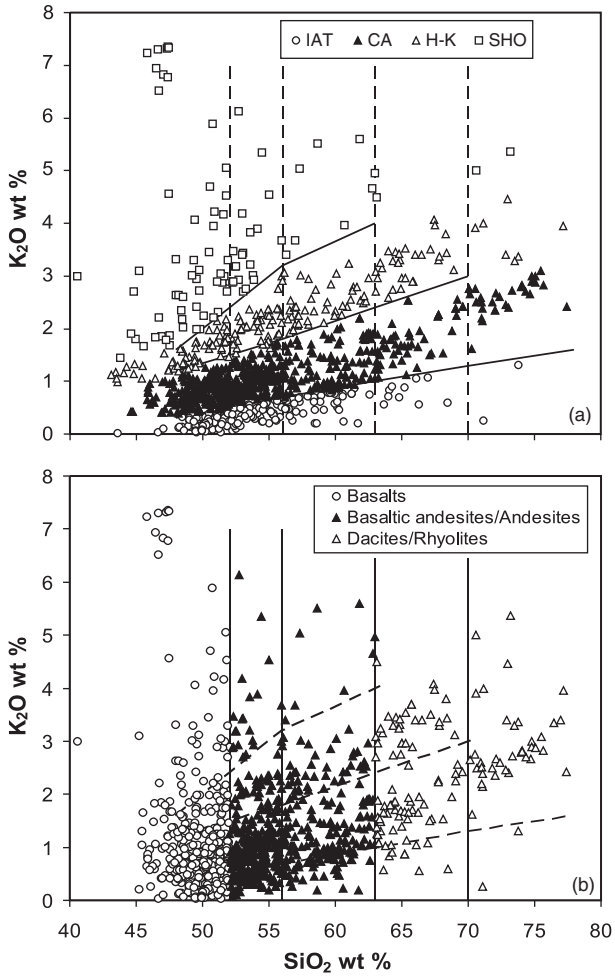

Fig. 5. K_2O–SiO_2 discrimination diagrams for the 1095 island arc analyses (Electronic Appendix A). Compositional fields are from Peccerillo & Taylor (1976). IAT, island arc tholeiite; CA, calc-alkaline; H-K, high-K calc-alkaline; SHO, shoshonite. (a) Rock series classification and (b) rock type classification for comparison with Fig. 6.

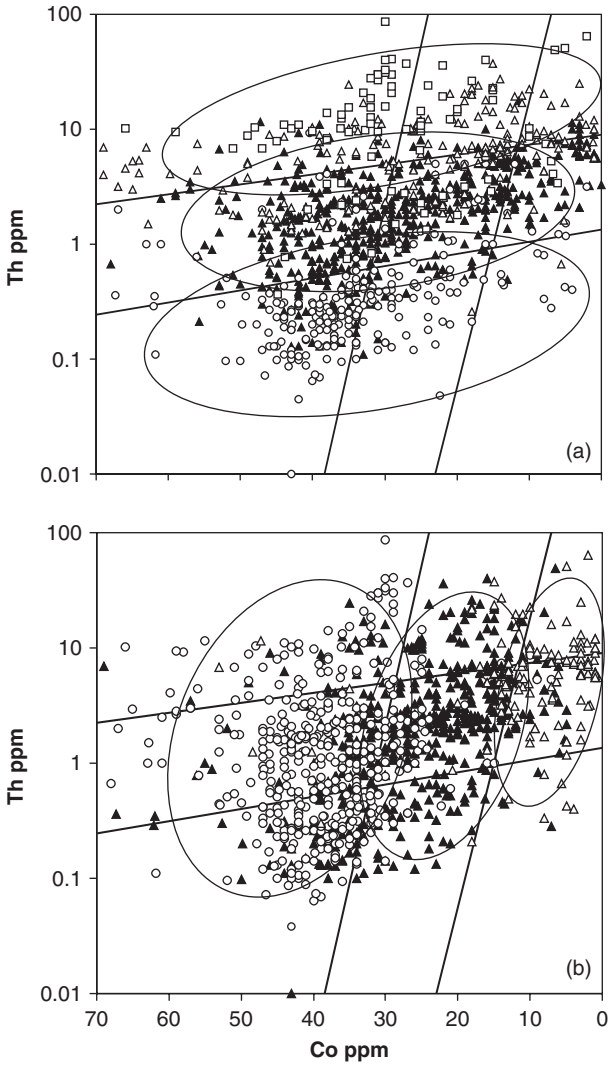

Fig. 6. Th–Co discrimination diagrams showing the 1095 arc lavas classified using Fig. 5. (a) Samples plotted as rock series; (b) samples plotted as rock type. Key as in Fig. 5. The 85% contour lines are also illustrated for each rock series and rock type.

Co probably account for a significant proportion of the 'missing' 20%. Also, as noted above, Th is not a perfect proxy for K, as it is usually not mobilized in a subduction zone at shallow depths. In addition, there are other complicating factors. For example, Co and SiO_2 are concentrated in different minerals and so are affected differently by crystal accumulation. None the less, it is unlikely that any diagram could precisely reproduce the K_2O–SiO_2 diagram and, as new and better data become available, it should be possible to improve the Th–Co diagram (Fig. 7).

Applying the diagram to the Jamaican samples reveals a change in arc chemistry from tholeiitic to calc-alkaline affinities. The Th–Co diagram indicates that the lowermost lavas have tholeiitic affinities and range in composition from basaltic andesites to dacites–rhyolites. The uppermost lavas have calc-alkaline affinities and range in composition from basalts to basaltic andesites (Fig. 8). These results are very similar to those obtained based on Fig. 3b and c, but now they may be achieved slightly more precisely and by a single proxy diagram rather than two diagrams.

CONCLUSIONS

(1) Because of the near-ubiquitous alteration and/or weathering of ancient volcanic rocks, it is useful to have immobile element proxy diagrams to replace conventional diagrams for rock classification. At present, at least one diagram (Zr/TiO_2–Nb/Y) can be used to replace the total alkali–silica (TAS) diagram. However, there is no immobile element equivalent for

Table 2: Classification of the training set (a) and the testing set (b) samples using the Th–Co discrimination diagram

(a) Classification of the training set

	Th–Co magma type			Sum	% correct
	IAT	CA	HK-SHO		
SiO_2–K_2O magma type					
IAT	193	45	1	239	81
CA	63	481	30	574	84
H-K/SHO	3	83	196	282	70
Average% correct					78
Average% correct for IAT and CA					82
	Th–Co magma type			Sum	% correct
	Basic	Intermediate	Acid		
SiO_2–K_2O magma type					
Basalt	375	56	3	434	86
Basaltic andesite–andesite	138	366	29	533	69
Dacite–rhyolite	5	26	97	128	76
Average% correct					77

(b) Classification of the testing set

	Th–Co magma type			Sum	% correct
	IAT	CA	HK-SHO		
SiO_2–K_2O magma type					
IAT	38	10	0	48	79
CA	5	28	2	35	80
H-K/SHO	0	0	11	11	100
Average% correct					86
	Th–Co magma type			Sum	% correct
	Basic	Intermediate	Acid		
SiO_2–K_2O magma type					
Basalt	26	8	0	34	76
Basaltic andesite–andesite	11	52	1	64	81
Dacite–rhyolite	0	2	22	24	92
Average% correct					83

In (a) and (b) the 'sum' columns denote the number of samples classified with the K_2O–SiO_2 diagram of Peccerillo & Taylor (1976). Data in the other columns are the number of samples classified in each category using the Th–Co diagram. The samples that classify correctly on the Th–Co diagram are also given as a percentage. The 'training set' is the data used to devise the diagram; 'the testing set' represents data 'held back' to test the method independently.

the Peccerillo & Taylor (1976) K_2O–SiO_2 diagram that is used to classify volcanic arc lavas.

(2) To achieve this, an immobile element proxy for K_2O must replicate its incompatibility, its enrichment above subduction zones and its enrichment during assimilation and fractional crystallization. Th is the most effective of the elements considered, being immobile up to lower amphibolite-facies metamorphism. Apart from arc volcanoes with a high shallow subduction component, K–Th diagrams show that Th replicates K_2O well.

(3) The immobile element proxy for SiO_2 must replicate its steady change from basic to acid compositions and its relative lack of variation in primary magmas.

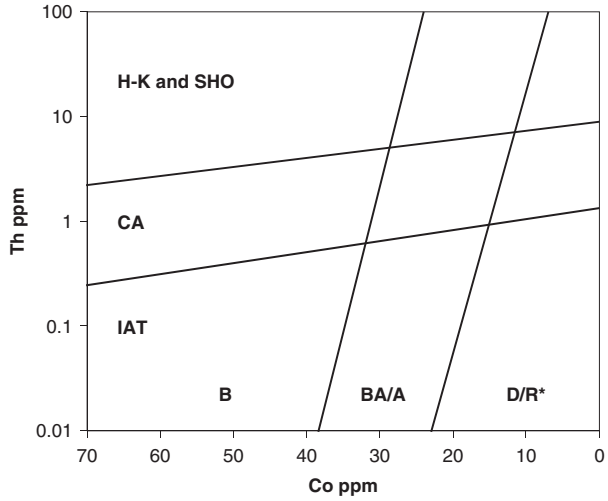

Fig. 7. The Th–Co discrimination diagram. B, basalt; BA/A, basaltic andesite and andesite; D/R*, dacite and rhyolite (* indicates that latites and trachytes also fall in the D/R fields). The field boundaries are: B–BA/A = (38·4, 0·01) to (24, 100); BA/A–D/R = (23, 0·01) to (7, 100); IAT–CA = (70, 0·245) to (0, 1·35); CA–H-K/SHO = (70, 2·2) to (0, 9).

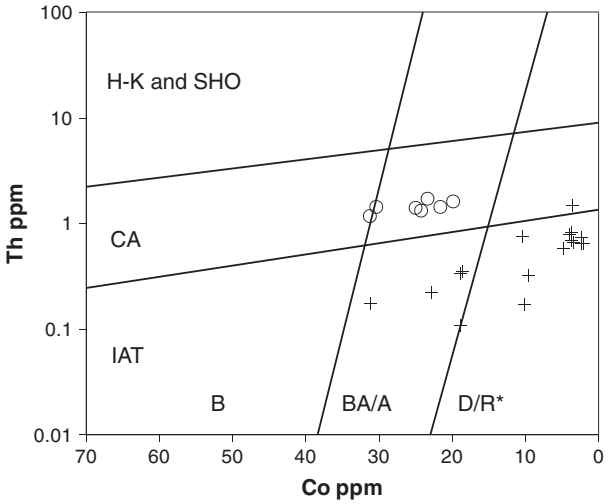

Fig. 8. Th–Co classification of the Devils Racecourse lavas. Key as in Fig. 2.

No incompatible element or element ratio accomplished this. However, the slightly compatible element Co did provide a good proxy, despite decreasing rather than increasing during fractional crystallization. It has some advantages over Zr/TiO_2 as a proxy, being less affected by Fe–Ti oxide accumulation and zircon crystallization.

(4) The resulting Th–Co classification diagram acts as the proxy for the K_2O–SiO_2 diagram. Fields drawn on the basis of 85% probability contours demonstrate that it is not possible to separate high-K calc-alkaline from shoshonitic samples, nor basaltic andesite from andesite or dacite from rhyolite samples with a high degree of confidence. However, a 'testing set' of samples not used in the original classification demonstrates that it can achieve *c.* 80% success rate in separating tholeiitic from calc-alkaline from high-K calc-alkaline plus shoshonite series, and in separating basalt from basaltic andesite plus andesite from dacite plus rhyolite rock types. Usefully, it is also topologically similar to the K_2O–SiO_2 diagram.

(5) This diagram is especially valuable for classification of lavas within tropical regions because of the more intense weathering, but works equally well with rocks that have undergone hydrothermal alteration and/or metamorphism. Retention of Co in iron and manganese oxyhydroxides and mafic metamorphic phases such as amphibole and chlorite ensures that Co is usually immobile. However, it should be stressed that, as with other immobile trace element discrimination and classification diagrams, tests for element immobility should always be carried out, and petrography and field evidence should be taken into account in any application. Moreover, as with other diagrams, the classification boundaries are not absolute but represent fields within which a particular rock type or volcanic series is the most probable interpretation. Nevertheless, the Th–Co plot provides a potentially useful projection for classifying altered volcanic arc lavas.

ACKNOWLEDGEMENTS

A.H. gratefully acknowledges receipt of a NERC PhD Studentship (NER/S/A/2003/11215). We thank Iain McDonald and Eveline DeVos for their analytical expertise in ICP-OES and ICP-MS at Cardiff University, and Martin Wolstencroft for his expertise in using the computer program Generic Mapping Tools (GMT). A special thank you must go to Arnott Jones, Ryan Ramsook, Ruth Liley and Vencott Adams for providing valuable help with fieldwork and logistics in Jamaica, and to Mike Widdowson for pointing me in the right direction at the beginning of the project. Constructive reviews by Edward Lidiak, Kaj Hoernle and Robert Trumbull significantly improved the manuscript.

SUPPLEMENTARY DATA

Supplementary data for this paper are available at *Journal of Petrology* online.

REFERENCES

Arculus, R. J. (2003). Use and abuse of the terms calcalkaline and calcalkalic. *Journal of Petrology* **44**, 929–935.

Becker, H., Jochum, K. P. & Carlson, R. W. (2000). Trace element fractionation during dehydration of eclogites from high-pressure

terranes and the implications for element fluxes in subduction zones. *Chemical Geology* **163**, 65–99.

Brenan, J. M., Shaw, H. F. & Ryerson, F. J. (1995). Experimental evidence for the origin of lead enrichment in convergent-margin magmas. *Nature* **378**, 54–56.

Burke, K., Coates, A. G. & Robinson, E. (1969). Geology of the Benbow Inlier and surrounding areas, Jamaica. In: Saunders, J. B. (ed.) *Transactions of the Fourth Caribbean Geological Conference*, Trinidad, 28 March–12 April, 1965, pp. 229–307.

Cann, J. R. (1970). Rb, Sr, Y, Zr and Nb in some ocean floor basaltic rocks. *Earth and Planetary Science Letters* **10**, 7–11.

Class, C., Miller, D. M., Goldstein, S. & Langmuir, C. (2000). Distinguishing melt and fluid subduction components in Umnak Volcanics, Aleutian Arc. *Geochemistry, Geophysics, Geosystems* **1**, paper number 1999GC000010.

Dosseto, A., Bourdon, B., Gaillardet, J., Allègre, C. J. & Filizola, N. (2006). Time scale and conditions of weathering under tropical climate: Study of the Amazon basin with U-series. *Geochimica et Cosmochimica Acta* **70**, 71–89.

Elliott, T. (2003). *Tracers of the Slab. Inside the Subduction Factory. American Geophysical Union, Geophysical Monograph* **138**, 23–45.

Floyd, P. A. & Winchester, J. A. (1975). Magma type and tectonic setting discrimination using immobile elements. *Earth and Planetary Science Letters* **27**, 211–218.

Floyd, P. A. & Winchester, J. A. (1978). Identification and discrimination of altered and metamorphosed volcanic rocks using immobile elements. *Chemical Geology* **21**, 291–306.

Govindaraju, K. (1994). Compilation of working values and samples description for 383 geostandards. *Geostandards Newsletter* **18**, 1–158.

Hildreth, W., Fierstein, J., Siems, D. F., Budahn, J. R. & Ruiz, J. (2004). Rear-arc vs. arc-front volcanoes in the Katmai reach of the Alaska Peninsula: a critical appraisal of across-arc compositional variation. *Contributions to Mineralogy and Petrology* **147**, 243–275.

Hill, I. G., Worden, R. H. & Meighan, I. G. (2000). Yttrium: The immobility–mobility transition during basaltic weathering. *Geology* **28**, 923–926.

Hynes, A. (1980). Carbonitization and mobility of Ti, Y and Zr in Ascot formation metabasalts, S.E. Quebec. *Contributions to Mineralogy and Petrology* **75**, 79–87.

Jackson, T. A. (1987). The petrology of Jamaican Cretaceous and Tertiary volcanic rocks and their tectonic significance. In: Ahmad, R. (ed.) *Proceedings of a Workshop on the Status of Jamaican Geology*, Kingston 14–16 March 1984, Geological Society of Jamaica, special issue. pp. 107–119.

Johnson, M. C. & Plank, T. (1999). Dehydration and melting experiments constrain the fate of subducted sediments. *Geochemistry, Geophysics, Geosystems* **1**, paper number 1999GC000014.

Keppler, H. (1996). Constraints from partitioning experiments on the composition of subduction-zone fluids. *Nature* **380**, 237–240.

Kessel, R., Schmidt, M. W., Ulmer, P. & Pettke, T. (2005). Trace element signature of subduction zone fluids, melts and supercritical liquids at 120–180 km depth. *Nature* **437**, 724–727.

Kuno, H. (1968). Differentiation of basalt magmas. In: Hess, H. H. & Poldervaart, A. A. (eds) *Basalts: The Poldervaart Treatise on Rocks of Basaltic Composition, 2.* New York: Interscience, pp. 623–688.

Kurtz, A. C., Derry, L. A., Chadwick, O. A. & Alfano, M. J. (2000). Refractory element mobility in volcanic soils. *Geology* **28**, 683–686.

Le Bas, M. J., Le Maitre, R. W., Steckeisen, A. & Zanettin, B. (1986). A chemical classification of volcanic rocks based on the total alkali–silica diagram. *Journal of Petrology* **27**, 745–750.

Le Bas, M. J., Le Maitre, R. W. & Woolley, A. R. (1992). The construction of the total alkali–silica chemical classification of volcanic rocks. *Mineralogy and Petrology* **46**, 1–22.

McCulloch, M. T. & Gamble, J. A. (1991). Geochemical and geodynamical constraints on subduction zone magmatism. *Earth and Planetary Science Letters* **102**, 358–374.

McDonald, I. & Viljoen, K. S. (2006). Platinum-group element geochemistry of mantle eclogites: a reconnaissance study of xenoliths from the Orapa kimberlite, Botswana. *Applied Earth Science (Transactions of the Institution of Mining and Metallurgy B)* **115**, 81–93.

Miller, D. M., Goldstein, S. & Langmuir, C. (1994). Cerium/lead and lead isotope ratios in arc magmas and the enrichment of lead in the continents. *Nature* **368**, 514–519.

Miyashiro, A. (1974). Volcanic rock series in island arcs and active continental margins. *American Journal of Science* **274**, 321–355.

Nakano, S. (1993). Ueno basaltic rocks I: Heterogeneous magmas at two monogenetic volcanoes. *Journal of the Japanese Association of Mineralogists, Petrologists and Economic Geologists (Ganseki Kobutsu Kosho Gakkai-Shi)* **88**, 272–288.

Nakano, S. (1994). Ueno basaltic rocks II: Chemical variation in the Kiso Province, to the south of the Ontake volcano. *Journal of the Japanese Association of Mineralogists, Petrologists and Economic Geologists (Ganseki Kobutsu Kosho Gakkai-Shi)* **89**, 115–130.

Pearce, J. A. & Cann, J. R. (1973). Tectonic setting of basic volcanic rocks determined using trace element analyses. *Earth and Planetary Science Letters* **19**, 290–300.

Pearce, J. A. (1976). Statistical analysis of major element patterns in basalts. *Journal of Petrology* **17**, 15–43.

Pearce, J. A. (1982). Trace element characteristics of lavas from destructive plate boundaries. In: Thorpe, R. S. (ed.) *Andesites.* Chichester: John Wiley, pp. 525–547.

Pearce, J. A. & Peate, D. W. (1995). Tectonic implications of the composition of volcanic arc magmas. *Annual Review of Earth and Planetary Sciences* **23**, 251–285.

Pearce, J. A. (1996). A users guide to basalt discrimination diagrams. In: Wyman, D. A. (eds) *Trace Element Geochemistry of Volcanic Rocks: Applications for Massive Sulphide Exploration. Geological Association of Canada, Short Course Notes* **12**, 79–113.

Pearce, J. A. & Parkinson, I. J. (1993). Trace element models for mantle melting: application to volcanic arc petrogenesis. In: Prichard, H. M., Alabaster, T., Harris, N. B. W. & Neary, C. R. (eds.) *Magmatic Processes and Plate Tectonics (I. G. Gass Memorial Volume). Geological Society, London, Special Publications* **76**, 373–403.

Peccerillo, R. & Taylor, S. R. (1976). Geochemistry of Eocene calc-alkaline volcanic rocks from the Kastamonu area, northern Turkey. *Contributions to Mineralogy and Petrology* **58**, 63–81.

Regelous, M., Collerson, K. D., Ewart, A. & Wendt, J. I. (1997). Trace element transport rates in subduction zones: evidence from Th, Sr and Pb isotope data for Tonga–Kermadec arc lavas. *Earth and Planetary Science Letters* **150**, 291–302.

Rickwood, P. C. (1989). Boundary lines within petrologic diagrams which use oxides of major and minor elements. *Lithos* **22**, 247–263.

Robinson, E., Lewis, J. F. & Cant, R.V. (1972). Field guide to aspects of the geology of Jamaica. *International Field Institute Guidebook to the Caribbean Island Arc System 1970.* Washington D.C.: American Geological Institute. 1–45, 1–4.

Roobol, M. J. (1972). The volcanic geology of Jamaica. In: Petzall, C. (ed.) *Transactions of the 6th Caribbean Geological Conference*, Margarita, Venezuela, 6–14 July 1971. pp. 100–107.

Savov, I. P., Ryan, J. G., D'Antonio, M., Kelley, K. & Mattie, P. (2005). Geochemistry of serpentinized peridotites from the Mariana Forearc–Conical Seamount, ODP Leg 125: Implications for the elemental recycling at subduction zones. *ıGeochemistry, Geophysics, Geosystemsı* **6**, paper number 2004GC000777.

Shervais, J. W. (1982). Ti–V plots and the petrogrenesis of modern and ophiolitic lavas. *Earth and Planetary Science Letters* **59**, 101–118.

Summerfield, M. A. (1997). *Global Geomorphology*. Singapore: Longman, pp. 129–144.

Sun, S.-s. & McDonough, W. F. (1989). Chemical and isotope systematics of oceanic basalts: implications for mantle composition and processes. In: Saunders, A. D. & Norry, M. J. (eds) *Magmatism in the Ocean Basins. Geological Society, London, Special Publications* **42**, 313–34542.

Trescases, J. J. (1973). Weathering and geochemical behaviour of the elements of ultramafic rocks in New Caledonia. Bulletin of Bureau of Mineral Resources, *Geology and Geophysics*, Canberra **141**, 149–161.

Winchester, J. A. & Floyd, P. A. (1976). Geochemical magma type discrimination: application to altered and metamorphosed basic igneous rocks. *Earth and Planetary Science Letters* **28**, 459–469.

Winchester, J. A. & Floyd, P. A. (1977). Geochemical discrimination of different magma series and their differentiation products using immobile elements. *Chemical Geology* **20**, 325–343.

Wood, D. A., Joron, J.-L. & Treuil, M. (1979). A re-appraisal of the use of trace elements to classify and discriminate between magma series erupted in different tectonic settings. *Earth and Planetary Science Letters* **45**, 326–336.